frontiers | Frontiers in Earth Science

TYPE Original Research
PUBLISHED 09 May 2023
DOI 10.3389/feart.2023.1171090

OPEN ACCESS

EDITED BY
Vlad Constantin Manea,
National Autonomous University of Mexico, Mexico

REVIEWED BY
Hossein Azizi,
University of Kurdistan, Iran
Nils Lenhardt,
University of Pretoria, South Africa

*CORRESPONDENCE
Lixin Wang,
wlxin@mail.cgs.gov.cn
Binhua Cao,
67980193@qq.com

RECEIVED 21 February 2023
ACCEPTED 17 April 2023
PUBLISHED 09 May 2023

CITATION
Wu F, Wang L, Huo Z, Liao J, Tang Y, Yang T, Li X, Wang S, Xiao H and Cao B (2023), Geochronology and geochemistry of the Late Jurassic-Early Cretaceous Sangxiu Formation volcanic rocks of the Chegu region, Southern Tibet.
Front. Earth Sci. 11:1171090.
doi: 10.3389/feart.2023.1171090

Geochronology and geochemistry of the Late Jurassic-Early Cretaceous Sangxiu Formation volcanic rocks of the Chegu region, Southern Tibet

Feng Wu[1], Lixin Wang[2,3]*, Zhitao Huo[1], Jia Liao[1], Yao Tang[1], Tao Yang[1], Xin Li[1], Shijie Wang[1], Hongji Xiao[4] and Binhua Cao[2,4]*

[1]Changsha General Survey of Natural Resources Centre, China Geological Survey, Changsha, China, [2]Yantai Center of Coastal Zone Geological Survey, China Geological Survey, Yantai, China, [3]School of Environmental Studies, China University of Geosciences, Wuhan, China, [4]School of the Earth Sciences and Resources, China University of Geosciences, Beijing, China

The evolution patterns of the Neo-Tethys Himalayas have been a major topic of research, particularly in the Neo-Tethys Ocean. The geological field investigations were conducted in the Late Jurassic-Early Cretaceous Sangxiu Formation in the Tsomei Longzi area of Tibet. A stratigraphic hierarchy of the Sangxiu Formation was established based on an analysis of the sedimentary lithology in this area. Based on the geochemical characteristics and chronology of the felsic-mafic volcanic rocks of the Sangxiu Formation, the genesis, tectonic background, and evolutionary pattern of the volcanic rocks of the Sangxiu Formation were revealed. Basalts, dolerite, and volcanic debris constitute the volcanic rocks of the Sangxiu Group in the Zhegu area. The Early Cretaceous Sangxiu Formation basalts were determined using SHRIMP zircon U-Pb ages of 141 ± 1 Ma and 142 ± 1 Ma. Volcanic rocks of the Sangxiu Formation, which are intraplate rifting products of the Late Jurassic-Early Cretaceous period, originated from the mantle and mixed with crustal materials. The rock type is an intraplate alkaline basalt that formed during the rifting activity of the passive continental margin extension. There was a crucial growth episode in the Neo-Tethys Ocean during the Late Jurassic and Early Cretaceous. The Neo-Tethys Ocean expansion from the Late Triassic to the Early Cretaceous was caused by a younger rifting along the passive continental edge rather than a continuation of the early Mid-Ocean Ridge development, thus demonstrating the expansion of the Neo-Tethys Ocean at various stages.

KEYWORDS

geochemistry, geochronology, Sangxiu formation, volcanic rocks, Southern tibet

1 Introduction

The Tethyan Himalayas are located in the northeastern part of the Ganges-Himalayan orogenic system (Hodges, 2000; Cawood et al., 2018; Cheng et al., 2022), between the Yarlung Tsangpo Suture Zone and the South Tibetan Dissociation System. It has a complex tectonic evolutionary history, including the rifting of the East Gondwana continent, Neo-Tethyan ocean evolution, and the plate collision between India and Eurasia. The Himalayan region, due to its high rates of physical weathering, generates significant amounts of

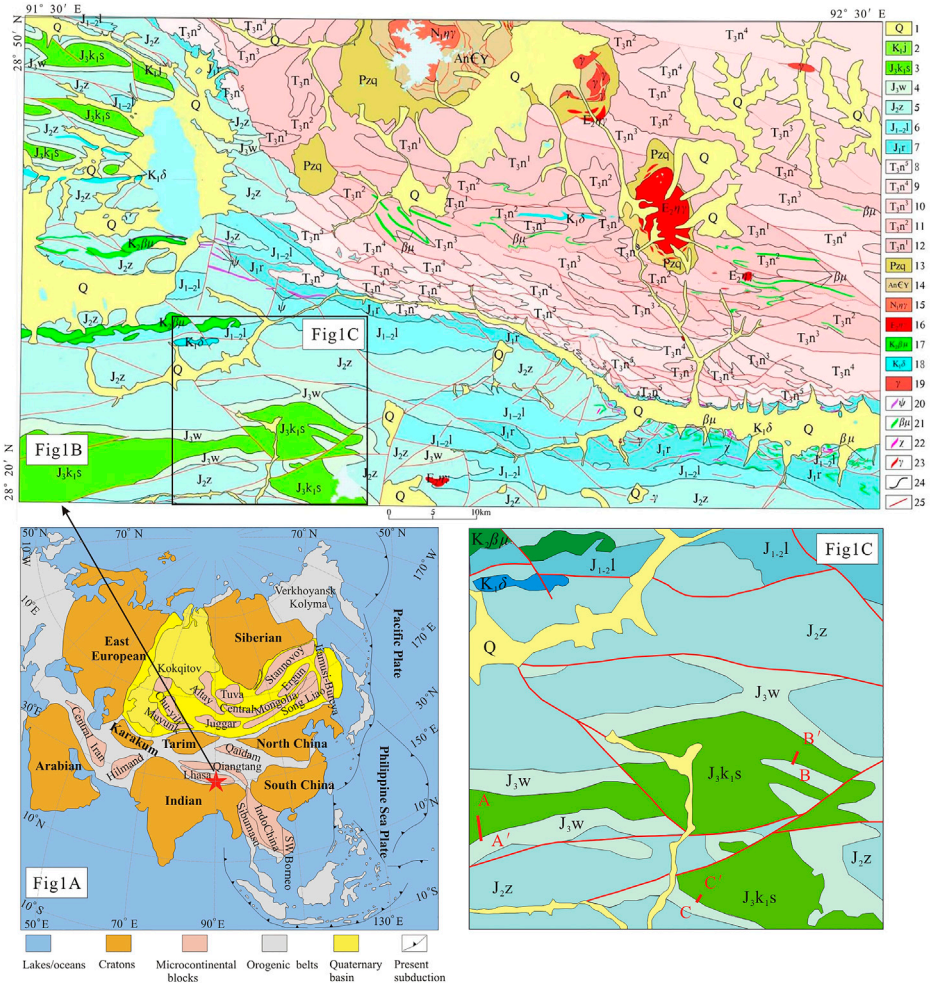

FIGURE 1
Geological sketch map and tectonic outline overview of the Zhegu-Gutui area in Tibet (Cawood et al., 2018). 1-Quaternary (fine gravel), sand, clay and glacial deposits; 2-Lower Cretaceous Kebula Formation; 3-Upper Jurassic and Lower Cretaceous Sangxiu Formation; 4-Upper Jurassic Vimy Formation; 5-Middle Jurassic Jurassic Middle and Lower Jurassic Luje Formation; 7-Lower Jurassic Ridang Formation; 8-Upper Triassic Neru Formation Section V; 9-Upper Triassic Neru Formation Section IV; 10-Upper Triassic Neru Formation Section III; 11-Upper Triassic Neru Formation Section II; 12-Upper Triassic Neru Formation Section I; 13-Paleozoic and Metasedimentary Qudegon Formation; 14-Metasedimentary Yaduzhara Group; 15-Neogene Miocene fine-grained dolomite diorite granite; 16-Paleocene Eocene black mica granite; 17-Late Cretaceous gabbro; 18-Early Cretaceous amphibolite; 19-granite; 20-ggabbro veins; 21-gabbro, diabase (porphyritic) veins; 22-lamprophyre; 23-granite (porphyritic) veins; 24-projected and measured geological boundaries; 25-projected and measured faults.

terrigenous detritus and organic carbon that are transported to the oceanic environment, which may exert a discernible impact on global climate change (Xu et al., 2021; Jiang et al., 2023). The Sangxiu Formation is widespread in central segments of the Tethyan Himalayas. It comprises interbedded volcano-sedimentary strata, varying in age from the Late Jurassic to the Early Cretaceous (Zhong et al., 2005; Zhu et al., 2009). The formation age, petrogenesis, and geodynamic background of the volcanic rocks in the Sangxiu Formation remain controversial. Early studies have examined the petrography, geochemistry, and mineralogy of the dacite in the Sangxiu Formation and proposed that magmatic activity is related to partial anatexis triggered by asthenospheric upwelling during intense rifting at the Himalayan passive continental margin (Zhong et al., 2005). However, combined with zircon U-Pb chronology, the Sangxiu volcanic rocks, which was formed at 133–142 Ma, may represent the initial stage of the separation of Greater India from southwestern Australia (Zhu et al., 2007; Dong et al., 2018; Tian et al., 2021). Further geochemical characteristics suggest that the dacite of the Sangxiu Formation formed during deep crustal melting in an intraplate extensional rifting environment, as part of the Comei-Bunbury Large Igneous Province, representing the products of early magmatism in the Kerguelen mantle plume (Zhu et al., 2009; Zhu et al., 2013).

The felsic volcanic rocks of the Sangxiu Group in the Yangzhuoyongzuo area have been studied, but not enough to show their overall characteristics (Tian et al., 2021). Understanding the chronology and petrogenesis of felsic-mafic volcanic rocks is not comprehensive enough to support the formation and evolution patterns of the Sangxiu Group. In this

study, we conducted a systematic field geological survey of the Late Jurassic-Early Cretaceous Sangxiu Formation in the Tsomei-Longzi area of Tibet. The sedimentary stratigraphy of the Sangxiu Formation in this area was delineated. Based on the geochemical characteristics and chronology of the felsic-mafic volcanic rocks of the Sangxiu Formation, the genesis, tectonic background, and evolutionary pattern of the volcanic rocks of the Sangxiu Formation were revealed. This study provides new material for the study of the felsic-mafic components of regional Late Jurassic-Early Cretaceous magmatism. Additionally, new evidences is provided for the study of the East Gondwana continental rifting event and the evolution of the Tethys-Himalayan tectonic domain.

2 Regional geological background

The Precambrian and Paleozoic metamorphic basement and continuously deposited Triassic, Jurassic, and Cretaceous covers are exposed in the study area (Figure 1), which is located in the Himalayan massif. The Precambrian Yaduzhara Group and the Paleozoic Quedegon Formation (Pzq) are upper greenschist to lower amphibolite facies. The Late Triassic Neyru Formation (T_3n) is a set of subdeep-sea slope complex lithic deposits represented by interbedded metamorphic feldspathic quartz-hybrid sandstone and sericite siltstone. The Jurassic system generally consists of a set of muddy siltstone, quartz sandstone, feldspathic sandstone, and limestone assemblages, representing a set of coastal-shallow shelf sedimentary facies locally interspersed with volcanic rocks such as dacite and basalt. The Early Jurassic Ridang Formation (J_1r) is characterized by black shale and thin grey-black sandstone interbedded with feldspathic quartz sandstone and limestone. The Early and Middle Jurassic Luge Formation ($J_{1\text{-}2}l$) is characterized by thin-bedded microcrystalline limestone interbedded with thin-middle grey-black calcareous shale and calcareous siltstone. The Middle Jurassic Chara Formation (J_2z) is characterized by dark gray mudstone and siltstone interbedded with dark gray to grey black thick giant thick basalt and dacite. The Late Jurassic Vimy Formation (J_3w) is dominated by quartz sandstone, siltstone, and black shale. The Late Jurassic-Early Cretaceous Sangxiu Formation (J_3-K_1s) is dominated by dark grey basalt, andesitic basalt, and basaltic volcanic conglomerate with a small amount of mud shale and siltstone. The Early Cretaceous Kebula Formation (K_1j) is a set of shallow shelf-coastal shallow marine facies mainly consisting of black shale, microcrystalline limestone, and grey siliceous rocks that gradually transition to feldspathic quartz sandstone and quartz sandstone.

The distributional characteristics of the stratigraphy in the study area are controlled by the fold structure (Figure 1). The stratigraphic extension direction, which is consistent with the regional fold line, is nearly east-west. The Sangxiu Formation is mainly distributed in the east-west and northwest-west directions of the regional complex oblique core. It is in conformable contact with the underlying grey-black and black shales of the Late Jurassic Vimy Formation (J_3w), surrounded by grey thin-bedded siltstone and fine sandstone. It was in conformable contact with the overlying microcrystalline limestone of the Early Cretaceous Kebula Formation (K_1j). The Sangxiu Formation was divided into three sections (III, II, and I) in the study area. Section 1; Section 3 contained more volcanic rocks, whereas Section 2 was mainly clastic.

Section 1 of the Sangxiu Formation (J_3-K_1s^1): The lithology is mainly dark grey thick-layered massive basalt, dark grey andesitic basalt, grey-black shale, and dark grey thin-layered siltstone. Grey-white medium- and thick-layered quartz sandstones and clastic-bearing quartz sandstones are occasionally observed, exhibiting volcanic eruptive phase deposition in a shallow coastal environment. The bottom is marked by basalt and andesitic basalt, which are in contact with the underlying Vermillion Formation. Pillow lava often develops at the bottom of the basalt (Figures 2A, B).

Section 2 of the Sangxiu Formation (J_3-K_1s^2): The lithology is mainly grey-black shale, dark grey siltstone, dark grey muddy siltstone interspersed with gray-green sandstone, and occasionally interspersed with light grey thin-bedded marl. Unstable yellow-green gravel-bearing graywackes developed lenticularly at the bottom. The scoured surface is displayed at the bottom of the gravel-bearing graywacke. The gravel in the graywacke consists of volcanic rocks, sandstone, and aragonite fossils, which generally show coastal marine facies during the volcanic activity interval (Figures 2C, D).

Section 3 of the Sangxiu Formation (J_3-K_1s^3): The lithology is mainly grey and grey-green basalt, basaltic volcanic breccia, grey thickly laminated calcareous glauconite-bearing fine-grained quartz sandstone, and dark grey siltstone with a small amount of light grey thin-layered marl. Generally, the neritic continental shelf-littoral neritic facies are well reflected during the volcanic eruption period. A few pore structures are observed in the basalt, and the breccia component (content 15%–25%) in the basaltic volcanic breccia is mainly basalt and andesitic basalt. The thickness of a single layer of basaltic volcanic breccia is 20–200 cm (Figures 2E, F).

The intrusive rocks in the study area are widely developed and are generally produced in the form of stocks and veins. They are mainly augite rock, diabase (gabbro), quartzite (diorite), muscovite granite, gneissic granite, granodiorite porphyry, and two-mica monzonitic granite (black mica). The intrusion ages are mainly Neoproterozoic, Early Cretaceous, and Paleocene (Jiang et al., 2006; 2007).

3 Lithological characteristics of volcanic rocks

The volcanic rocks of the Sangxiu Group are mainly lavas with cryptocrystalline vitreous structures. Pore and amygdaloidal filling structures developed in these volcanic rocks, with occasional flow structures, pillow structures, and local columnar joints. The rock types include altered amygdaloid, basalt, andesitic, and volcanic breccia.

3.1 Amygdaloidal basalt

The rock developed porphyritic and intergranular matrix structure. Its porphyritic crystals are plagioclase and pyroxene with a small amount of amygdaloids (Figure 3A). This rock is

FIGURE 2
Field morphological characteristics of volcanic rocks of the Sangxiu formation in the Tsomei-Longzi area, Tibet. **(A, B)**: Section I of the Sangxiu Formation; **(C, D)**: Section II of the Sangxiu Formation; **(E, F)**: Section III of the Sangxiu Formation.

dominated by plagioclase (46%), pyroxene (40%), pyroxene phenocrysts (4%), and metallic minerals (2%). The plagioclase phenocryst presents a semi-automorphic, tabular morphology with grain dimensions spanning from 0.1 to 0.3 mm. The pyroxene phenocryst exhibits a semi-automorphic, columnar habit with granular textures and grain sizes ranging from 0.1 to 0.2 mm. Pyroxene is an anhedral crystal grain with a size of 0.02–0.05 mm. Metal minerals are irregularly and locally distributed, with a 2% content.

3.2 Pore-like andesitic basalt

The rock mainly consists of microscopic semi-automorphic plagioclase with grain sizes ranging from 0.12–0.25 mm, undirectedly intertwined (Figure 3B). The plagioclase grains were filled with yellow amorphous vitreous with devitrified crystals between them. As a result of interwoven intersertal and amygdaloidal structures, the rock developed rounded and elliptical pores with chalcedony walls and cores filled with carbonate. Plagioclase (62%) is a self-shaped plate bar-like mineral that is intertwined to form a lattice. Amorphous substances (26%) are fibrous and devitrified. Carbonate (3%) was mainly formed in stomata. Chalcedony (4%) is mainly distributed on stomatal walls. Opaque titanium-iron oxide (5%) has an irregularly granular and scattered distribution.

3.3 Dolerite

The rock is mainly composed of irregular lattices of 0.2–0.6 mm grain size euhedral lath-shaped plagioclase (Figure 3C), which is filled with fine pyroxene and opaque titanium iron oxides. The intergranular texture forms a diabasic texture. The rocks have locally developed pores filled with chlorite and calcite. Pyroxene (44%) is mostly chloritized, short columnar, granular, and colorless. Titanium iron oxide (4%) is a plate-shaped and anhedral granular. Chlorite (2%) is a blade-like aggregate that fills rock pores. Carbonate (1%) is anhedral granular and fills rock pores.

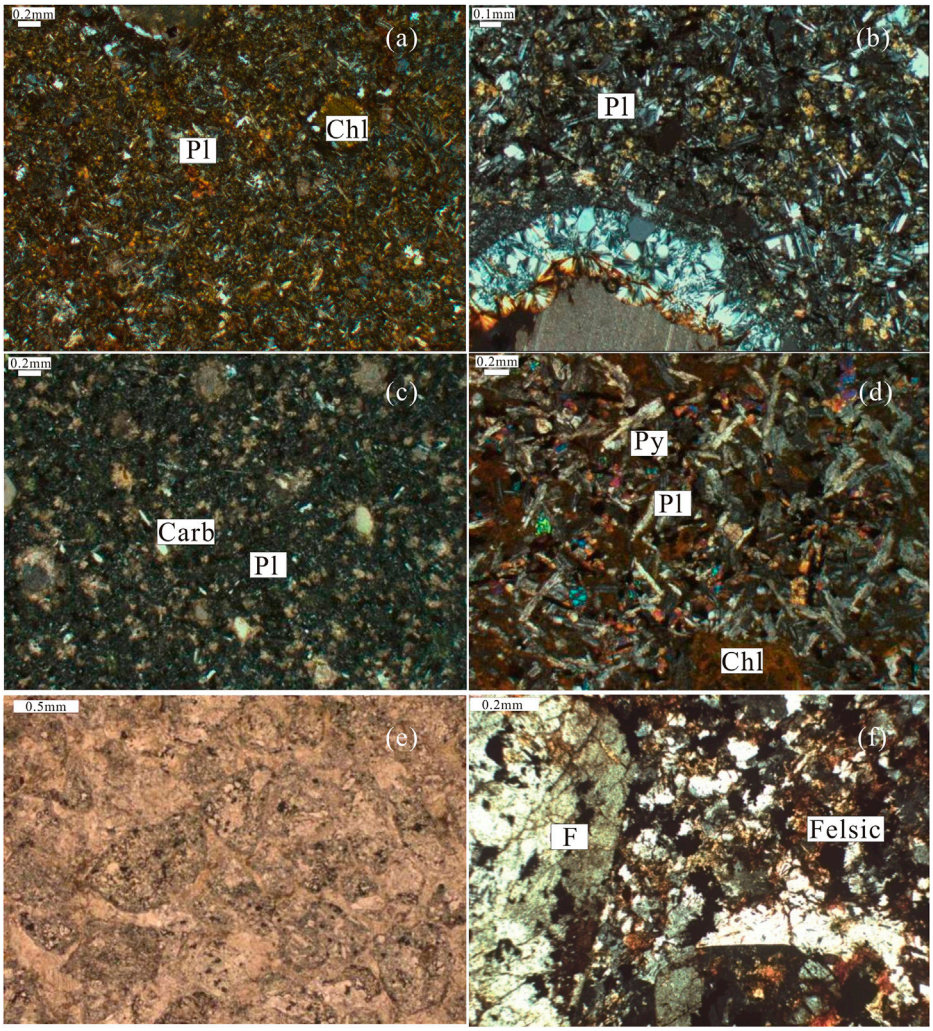

FIGURE 3
Microscopic features of volcanic rocks of the Sangxiu formation in the Tsomei-Longzi area, Tibet. **(A)**. Amygdaloidal basalt; **(B)**. Porous andesitic basalt; **(C)**. Dolerite; **(D)**. Andesitic volcanic breccia; **(E)**. Detritus sedimentary breccia tuff; **(F)**. Dacite. Pl: plagioclase. Chl: Chlorites. Carb: carbonate. Py: pyroxene. F: feldspar.

3.4 Andesitic volcanic breccia

The rock is mainly composed of randomly distributed andesitic breccias and angular fragments of different sizes. The fragments were metasomatized by microcrystalline calcite, volcanic ash, volcanic dust, and other cements. The rocks exhibit a volcanic breccia configuration. Andesite breccias and fragments (75%) have varying grain sizes of 0.2–20 mm and are basically angular with a small amount of long columnar plagioclase and a maroon amorphous substance in the breccias (Figure 3D). Microcrystalline calcite (18%) is microcrystalline and granular, with volcanic dust and ash. Volcanic ash and dust (7%) are microscopic angular fragments of volcanic amorphous minerals with particle sizes <0.02 mm.

3.5 Detritus sedimentary breccia tuff

The rock had a sedimentary breccia tuff structure (Figure 3E). The main components of the detritus were rhyolitic conglomerate debris, rhyolitic debris, and small amounts of limestone and feldspar crystal debris. The breccia is angular and subangular, and the gap-filling material is calcite. Calcite with particle sizes of 0.3–1 mm partly metasomatized rhyolitic debris (50%). Rhyolitic conglomerate debris (13%) has a general grain size of 2–3 mm, and was partially metasomatized by calcite. The feldspar crystals were partially metasomatized by calcite. Limestone debris: mainly subelliptical, locally visible, content of 1%. Calcite: irregular, generally 0.06–0.3 mm particle size, unevenly distributed between the debris, content of 35%.

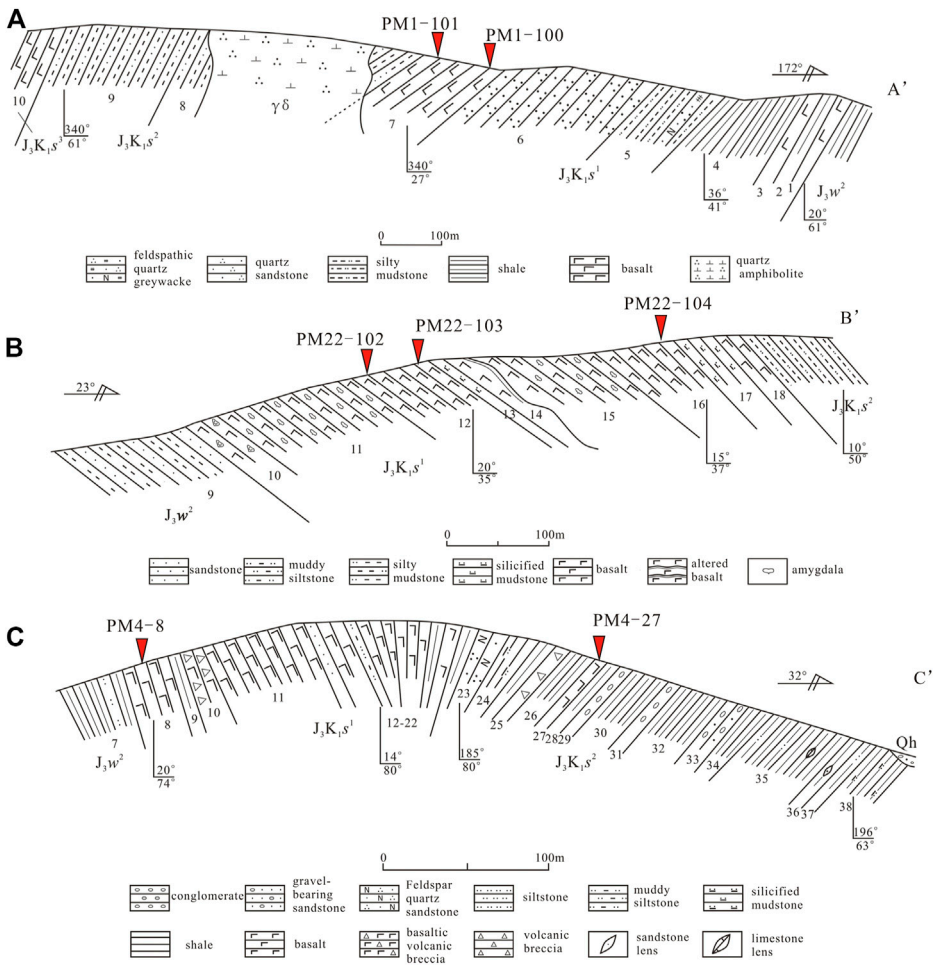

FIGURE 4
Measured stratigraphic sections and sampling locations of the Sangxiu formation in the Tsomei-Longzi area, Tibet. Profiles **(A, A')**, **(B, B')**, and **(C, C')** are shown in Figure 1C.

3.6 Dacite

(Figure 3F) The rock is mainly composed of anhedral semiautomatic quartz (1–2.5 mm), irregular platy bar-like plagioclase, potassium feldspar porphyry, felsic matrix, and opaque iron oxide. The rock has a porphyritic structure with a matrix of felsitic texture and a microscopic poikilitic structure. Quartz (4%) was porphyritic and rounded, with a wide melting corrosion edge around the periphery. Plagioclase: content of approximately 15%, porphyritic, irregular plate bar-shaped, with corroded periphery. Potassium feldspar (5%) was porphyritic, irregular, platy bar-shaped, and anhedral granular. Felsic matrix (70%) is characterized by felsitic texture, sericitization, and clayification. Iron oxide matrix (6%): irregularly granular, more uniformly dispersed, or distributed in the rock microfractures.

4 Samples and analysis methods

In this study, nine representative basaltic samples were collected from the Sangxiu Formation in the Tsomei-Longzi area of Tibet. Two samples (PM1-100 and PM1-101) were collected from the upper Section 1 (J_3-K_1s^1) of the Sangxiu Formation in the A-A' profile (Figure 4). Three samples (PM22-102, PM22-103, and PM22-104) were collected from the middle and upper parts of Section 1 (J_3-K_1s^1) of the Sangxiu Formation in profile B-B'. Two samples (PM4-8 and PM4-27) were obtained from the lower part of Section 1 (J_3-K_1s^1) of the Sangxiu Formation in profile C-C'. To ensure that the samples were fresh and representative, good outcrops and non-metamorphic areas were selected for collection during the sampling process. Zircon U-Pb radioisotope dating was performed for two basalt samples (PM4-8 and PM4-27) from upper Section 1 of the Sangxiu Formation (J_3-K_1s^1) in the C-C' profile. Subsequently, bulk major and trace element analyses combined with zircon U-Pb radioisotope dating were performed on seven samples.

Zircon grains were extracted using conventional heavy liquid and magnetic techniques and purified by hand-picking under a binocular microscope at the Beijing Geoanalysis Company Limited. The zircon grains for each sample were mounted in epoxy resin and polished in the center. All zircon grains were photographed under transmitted light, reflected light, and cathodoluminescence to identify their morphology and internal structures, and select

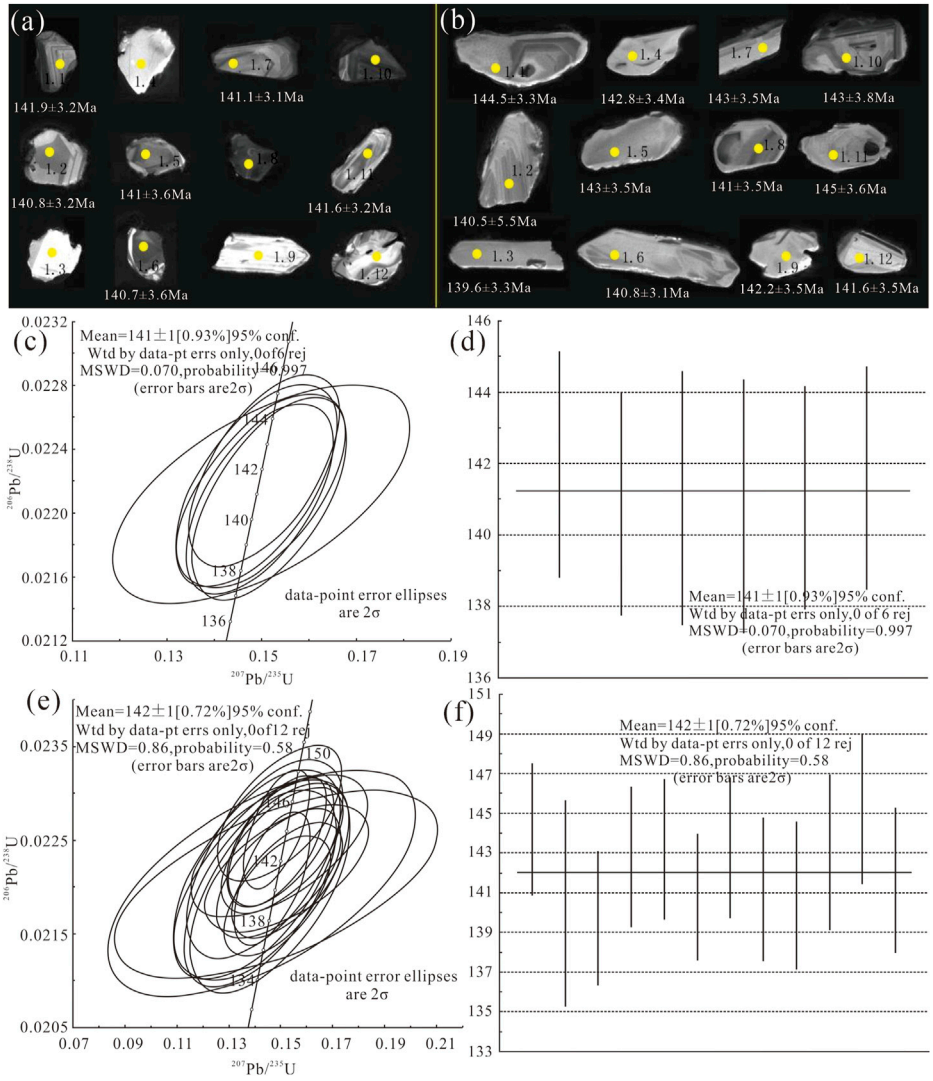

FIGURE 5
Zircon cathodoluminescence (CL) image [**(A)**: sample PM4-8. **(B)** sample PM4-27] and U-Pb concordia ages and data outlier characteristics **(C,D)** sample PM4-8. **(E,F)** sample PM4-27).

suitable crystals and analytical points. Zircon U–Pb isotopic and trace element analyses were synchronously performed on a Geo-Las2005 laser-ablation system attached to an Agilent 7500 a inductively coupled plasma mass spectrometer (ICP-MS) at the Wuhan Sample Solution Analytical Technology Company Limited. All analyses were conducted with a beam diameter of 30 μm and a 10-Hz repetition rate. Every set of five zircons was followed by an analysis of zircon standard 91,500 with age of 1,065 Ma. The detailed analytical technique is the same as that described by Liu et al. (2010). Concordia diagrams, weighted average age calculations, and probability density plotting were conducted using the Isoplot software.

The whole-rock geochemical analyses were conducted at the Southwest Institute of Metallurgical Geology, Ministry of Metallurgical Industry. The rock samples were crushed and powdered to 200 mesh using an agate mill. X-ray fluorescence spectrometry was used to analyze the major elements using an Axios mAX instrument, and the trace elements were analyzed using a Nex-LON300xICP-MS ICP–MS apparatus. The analytical precision was generally better than 5% for major and trace elements; the detection limit was less than 0.01 wt% for major elements and mostly less than 2 ppm for trace elements; and the relative standard deviation was below 1% for major elements and below 10% for trace elements. These results reflect the geochemical characteristics, magmatic source area properties, and diagenetic age of the basaltic rocks of the Sangxiu Formation in the study area.

5 Results

5.1 Zircon U-Pb age

The zircon shot locations were presented in Figure 5. The zircon grains are pale yellow, colorless, transparent, and self-semi-

10.3389/feart.2023.1171090

TABLE 1 Results of bulk major elements (%) analysis of the Sangxiu formation basalts in the Tsomei-Longzi area, Tibet. LOI: loss on ignition.

Samples	PM1-100	PM1-101	PM22-102	PM22-103	PM22-104	PM1-23	PM4-27
SiO_2	49.36	49.47	52.84	51.68	53.32	50.49	43.20
Al_2O_3	13.11	12.93	12.51	13.52	15.63	13.58	17.11
Fe_2O_3	6.76	5.11	3.64	3.50	5.74	6.33	3.43
FeO	6.17	8.10	7.65	6.20	0.96	5.95	9.66
TiO_2	4.57	4.98	3.92	3.91	4.00	4.37	4.08
CaO	6.11	5.99	5.29	7.68	4.22	5.76	6.08
MgO	4.51	5.08	5.56	5.07	2.92	4.53	2.62
MnO	0.189	0.192	0.160	0.138	0.114	0.154	0.081
K_2O	2.21	0.83	0.28	1.10	1.64	1.64	0.03
Na_2O	3.91	3.33	4.54	2.93	5.17	4.40	5.79
P_2O_5	0.64	0.41	0.45	0.57	0.61	0.58	0.70
LOI	1.22	2.36	2.07	2.42	3.27	1.50	6.89
A/CNK	0.65	0.74	0.72	0.67	0.87	0.69	0.83
SI	19.26	22.64	25.66	26.97	18.07	19.93	12.17
A.R	1.93	1.56	1.74	1.47	2.04	1.91	1.67
σ	5.18	2.25	2.15	1.65	3.45	4.41	11.09

automorphic, with a few anhedral grains. The zircon morphology is long, columnar, short, equiaxed, and irregular, with aspect ratios ranging from 1:1 to 1:3. Zircon concordia diagrams and outlier characteristics indicate that the crystallization ages of zircon in the two basalt samples were 141 ± 1 Ma (PM4-8) and 142 ± 1 Ma (PM4-27), respectively (Figure 5).

5.2 Major element characteristics

The average content of SiO_2 and Al_2O_3 is 52.25 wt% and 14.62 wt%, respectively. A/CNK ranged from 0.65 to 0.83, with an average of 0.74, belonging to the aluminum series. K_2O+ Na_2O was 4.18–7.07 wt%, with a mean value of 5.61 wt%. Rittman index (σ) of three samples was >3.3 (alkaline series), one sample (PM4-27) was 11.09 (super alkaline series), and the other three samples were <3.3 (calcium-alkaline series). Overall, the Sangxu Formation volcanic rocks had a higher Rittman index (σ) than the regional Neyru and Chara Formations (Table 1). The average TiO_2 content was 4.43 wt%. In the Nb/Y-Zr/TiO_2 diagram, most of the samples were cast near the alkaline basaltic region (Figure 6A). The alkalinity rate (A.R) ranged from 1.56 to 2.04, with a mean of 1.76. In the SiO_2-A. R variogram, one cast sample fell into the over alkaline zone, while five cast samples fell into the alkaline zone and nearby areas (Figure 6B). The solidification index ranged from 12.17 to 26.97 with an average value of 20.67 (Table 1), indicating a low degree of magmatic separation and crystallization of the volcanic rocks. The CIPW standard mineral combination was Q + Or + Di + Hy + An, which is a SiO_2 saturated type.

5.3 Rare earth and trace element characteristics

The rare earth elements (REE) contents and characteristic parameters of the Late Jurassic-Early Cretaceous volcanic rocks in the study area are listed in Table 2. The total rare earths (∑REE) content was 264.14 μg/g, similar to that of the Middle Jurassic basalts, but higher than that of the Late Triassic basalts. Eu had a weak positive anomaly (δEu > 1.02), which was explained by the Eu distribution in the Ca-rich plagioclase in the basalts (Sanematsu et al., 2011). Eu is thought to be found in the volcanic glass of some nepheline-bearing alkali basalts. These findings show that if REE were dispersed to the ion-adsorption portion by laterization of the basalt, alkali basalt might be a parent rock for REE deposits, especially light REE containing Eu. The rock was characterized by a slight Ce deficit, with δCe averaging 0.93. The average value of $(La/Yb)_N$ between light and heavy rare earths was 8.17, indicating a high degree of fractionation. The distribution pattern of REE normalized by spheroidal meteorites was right-skewed (Figure 7), with $(Ce/Yb)_N$ ranging from 5.47 to 8.42 and $(La/Sm)_N$ ranging from 1.81 to 2.64. Both characteristic parameters were greater than 1, reflecting a high degree of fractionation between light rare earths and heavy rare earths, and between light rare earths. The original mantle-standardized spider web diagram of trace elements in the volcanic rocks (Figure 7) was drawn according to

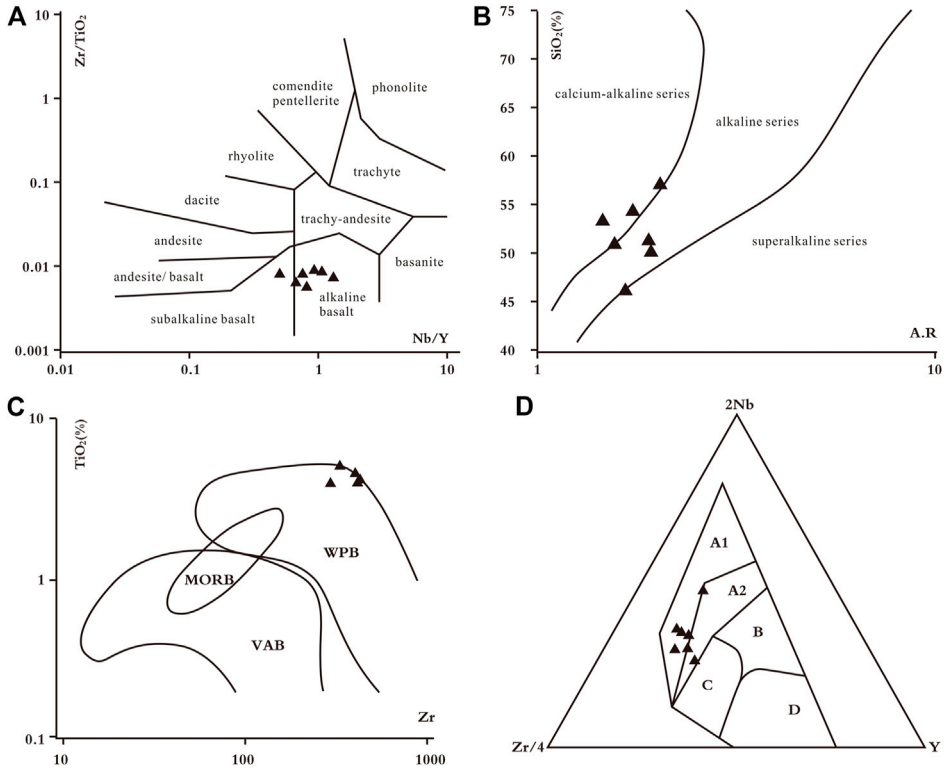

FIGURE 6
Geochemical discrimination plots for the volcanic rocks of the Sangxiu formation (Pearce and Norry, 1979; Vermeesch, 2006; Li et al., 2013; Pál-Molnár et al., 2015; Cheng et al., 2022). **(A)**. Nb/Y-Zr/TiO_2 diagram; **(B)**. SiO_2-A.R discrimination diagram; **(C)**. Zr-TiO_2 diagram; **(D)**. Nb-Zr-Y triangle discrimination diagram. WPB: intraplate basalts; MORB: mid-ocean ridge basalts; VAB: volcanic arc basalts; A1+A2: intraplate alkaline basalts; A2 + C: intraplate tholeiitic basalt; **(B)** P-type MORB; **(D)** N-type MORB; C+D: volcanic arc basalts.

the results of the trace element analysis (Table 3). Among the large-ion lithophile elements, Ba was enriched, whereas K, Sr, and Rb were depleted. Among the high-field-strength elements, Ta was enriched, Zr and Hf were relatively enriched, and Nb was slightly deficient. Therefore, the mantle was the magma source and where continental crustal materials were mixed. The Late Jurassic-Early Cretaceous volcanic rocks have many similarities with the Middle Jurassic volcanic rocks, reflecting their similar tectonic backgrounds.

6 Discussion

6.1 Age of magmatism in the Sangxu formation

The Early Cretaceous magmatic eruptions in the eastern Tethys Himalayas were large in scale and short in duration, covering more than 50,000 km^2 (Qiu, 2011), and their time period was mainly concentrated at 133–136 Ma (Tong et al., 2003; Zhu et al., 2005a; Zhu et al., 2005b; Jiang et al., 2006; Tong et al., 2007; Zhu et al., 2009). The basaltic rocks of the present zircon dating sample were collected from Section 1 of the Sangxiu Formation. Section 3 of the Sangxiu Formation has also developed basaltic rocks of varying thicknesses. Therefore, there were at least two phases of volcanic activity in the Late Jurassic-Early Cretaceous of the Zhegu area. The chrysolite fossils found in the muddy siltstone of the Chara Formation (J_2z), which formed earlier than the Sangxu Formation, were identified as *Macrocephalites* spp. Of the Middle Jurassic age (Jain, 2019). The bivalve fossils were identified as *Oxytoma* sp., dating from the Late Jurassic to Middle Cretaceous (Crame, 1996; Hryniewicz et al., 2015). Thus, the high-precision zircon harmonization ages of 141 ± 1 Ma and 142 ± 1 Ma obtained in this study indicated that the volcanic rocks of the Sangxiu Formation formed in the Zhegu area during the Early Cretaceous.

6.2 Geotectonic setting of the basaltic rocks of the Sangxiu formation

In the Zr-TiO_2 tectonic discrimination diagram (Pearce and Norry, 1979), all samples fell into an intraplate tectonic setting (Figure 6C). In the Nb-Zr-Y tectonic discrimination diagram, six samples fell into the zone A1, while one sample fell into zone A2. In contrast to Middle Jurassic basalts, the volcanic rocks of the Sangxiu Formation are intraplate alkaline basalts (Figure 6D). Another characteristic of the Sangxiu Formation basalt, which indicates alkaline basalts, is that the TiO_2 content of the major element is much higher than 2 wt%. In the spider diagram of trace elements normalized to the primitive mantle, Nb shows weak negative anomalies (Figure 7), indicating limited mixing of crustal materials.

10.3389/feart.2023.1171090

TABLE 2 Analytical results and characteristic parameters of bulk rare earth elements (10^{-6}) in basaltic rocks of the Sangxiu formation, Tsomei-Longzi area, Tibet.

Samples	PM1-100	PM1-101	PM22-102	PM22-103	PM22-104	PM1-23	PM4-27
Y	50.26	36.06	33.59	39.39	35.04	52.62	38.57
La	47.05	25.49	23.7	32.9	43.31	54.96	43.82
Ce	98.01	55.78	52.8	70.63	90.33	104.07	89.56
Pr	13.3	7.94	7.8	9.8	11.71	14.33	12.84
Nd	57.43	36.04	35.26	43.8	49.92	60.45	56.18
Sm	12.51	8.34	8.42	10.05	10.9	13.42	12.92
Eu	6.09	2.67	2.72	4.53	3.42	5.14	3.71
Gd	10.79	7.2	7.08	8.27	8.82	11.4	10.15
Tb	1.89	1.32	1.27	1.47	1.49	1.96	1.66
Dy	10.71	7.64	7.06	8.5	7.86	10.59	8.41
Ho	2.06	1.48	1.35	1.68	1.49	2.17	1.61
Er	5.43	3.87	3.55	4.29	3.84	5.47	4.02
Tm	0.78	0.52	0.49	0.62	0.56	0.83	0.59
Yb	4.27	2.83	2.62	3.41	2.98	4.41	3.12
Lu	0.62	0.42	0.39	0.52	0.42	0.73	0.43
∑REE	321.22	197.6	188.07	239.85	272.08	342.55	287.58
δEu	1.56	1.03	1.05	1.47	1.03	1.24	0.96
δCe	0.95	0.95	0.95	0.95	0.96	0.89	0.91
La_N/Yb_N	7.90	6.46	6.49	6.92	10.42	8.94	10.07
Ce_N/Yb_N	6.37	5.47	5.59	5.75	8.42	6.55	7.97
La_N/Sm_N	2.42	1.97	1.81	2.11	2.56	2.64	2.18
Gd_N/Yb_N	2.09	2.1	2.23	2.01	2.44	2.13	2.69

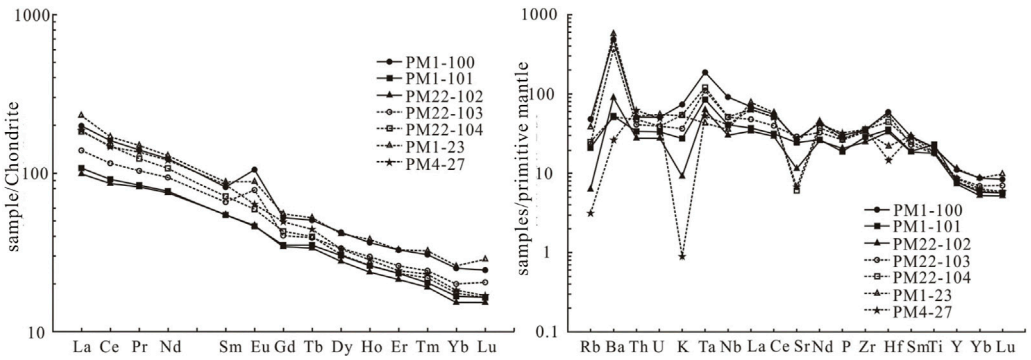

FIGURE 7
Chondrite—normalized REE and Primitive-mantle-normalized trace element patterns for the volcanic rocks of the Sangxiu formation.

The main rock assemblages of the Sangxiu Formation in the study area are shale and siltstone. Occasional grey-white medium- and thick-bedded quartzose sandstones and detritus-bearing quartzose sandstones interbedded with basalt are observed in the Sangxiu Formation. The emergence of pillow basalt in conformable contact with the underlying strata marks the bottom part. Oblique,

10.3389/feart.2023.1171090

TABLE 3 Results of bulk trace element analysis of basaltic rocks of the Sangxiu formation in the Tsomei-Longzi area, Tibet (10^{-6}, 10^{-9} for Au).

Samples	PM1-100	PM1-101	PM22-102	PM22-103	PM22-104	PM1-23	PM4-27
Cr	66.39	30.58	43.24	91.56	53.09	59.59	14.2
Ni	52.38	20.49	33.64	60.88	32.26	66.79	15.93
Co	60.87	52.24	54.94	50.1	48.63	37.2	32.51
Rb	30.49	13.19	4.04	14.87	15.68	24.58	1.98
Sr	573.7	505.8	245	612	128.4	533.9	141.6
Ba	3,399	372.9	634.5	2,552	356.1	4,078	183.8
Sc	24.08	23.02	24.04	20.68	21.19	23.11	15.47
Nb	65.02	29.19	22.03	36.46	36.49	25.99	28.98
Ta	7.62	3.46	2.59	4.47	4.92	1.78	2.18
Li	13.28	28.32	19.29	26.52	21.6	14.93	60.11
Zr	388.15	319.7	283.59	395.19	396.3	386	403
U	1.06	0.7	0.6	0.82	0.8	1.14	1.03
Th	4.39	2.86	2.4	3.49	4.08	4.47	5.27
W	3.71	18.18	1.62	3.99	5.15	7.11	1.46
Sn	3.78	7.57	2.21	2.47	2.54	3.38	3.13
Cu	43.29	42.35	23.19	33.51	17.51	80.55	47.88
Pb	17.12	27.54	17.02	27	15.58	6.9	8.28
Zn	131.4	149.8	123.7	108	122.4	163	184.4
Au	0.66	0.75	0.57	0.71	0.79	0.81	0.62
Hf	18.26	10.99	10.36	17.06	13.77	6.89	4.46
V	344.4	243.1	287.6	268.1	277.6	324.2	300.5

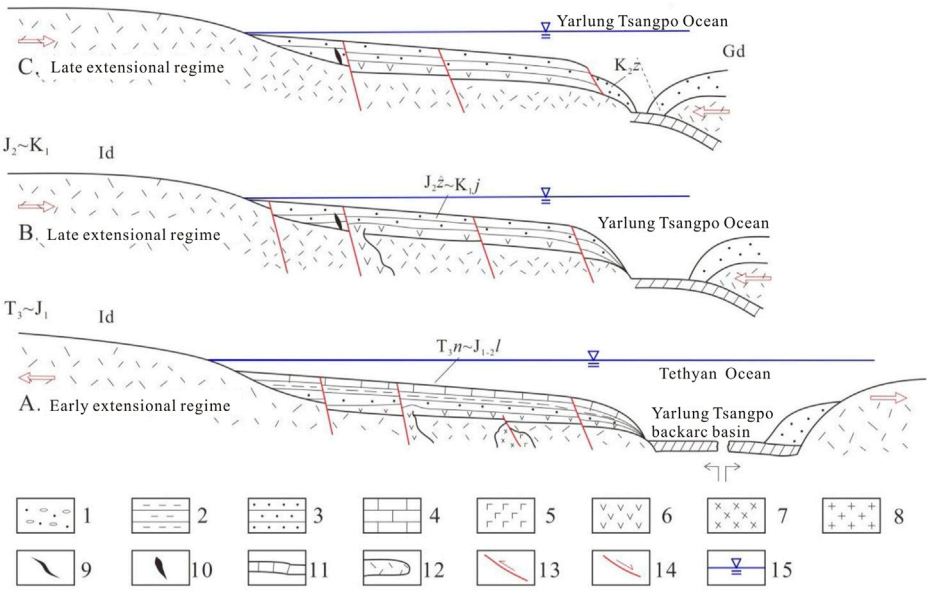

FIGURE 8
Geodynamic mode of Zhegu Area. 1. Sediment in river and lake facies; 2. Mudstone; 3. Sandstone; 4. Limestone; 5. Basalt; 6. Volcanic rock; 7. Diabase (porphyritic) rock; 8. Granite; 9. Intermediate-basic dike; 10. Ophiolite and basaltic veins; 11. Oceanic crust; 12. Continental crust; 13. Normal faults; 14. Thrust faults; 15 sea level; Id. The Indian massif; Gd. The gondwana massif. The geological evolution sequence follows the order of **(A–C)**.

low-angle oblique, and parallel laminations have been developed. Therefore, the Sangxiu Formation may have developed in a rift valley eruption and coastal-shallow shelf environment.

In summary, the Late Jurassic-Early Cretaceous volcanic rocks, which are intraplate rifting products, were formed in the mantle through the mixing of crustal materials. The rock type is intraplate alkaline basalt, which was formed during the extensional rifting activity of the passive continental margin. Compared with other volcanic rocks in the study area, it is characterized by higher TiO_2 and K_2O contents, a feature that clearly distinguishes it from the Late Triassic tholeiitic basalts. The latest active volcanic rocks have the highest total alkali content and geochemical characteristics, similar to those of the Middle Jurassic volcanic rocks. This indicates that the volcanic rocks of these two periods may have had similar magmatic origins and tectonic environments. Both may have been products of eruptions from different periods.

6.3 Stage of shelf rift

From the Middle to Late Permian, the study region was in an extensional continental margin tectonic setting, and basaltic magmatic activity persisted until the Cretaceous (Figure 8). The study region remains in a relatively stable paleocontinental margin basin tectonic setting. Owing to the influence of the Southern Tibetan Dissociation System, the Early and Middle Triassic strata are generally absent, and only the Late Triassic strata have been preserved in the study region. A large number of bed-parallel and bed-vertical basaltic gabbro and basalt lavas in the Triassic slates may represent a tectonic environment of crustal extension and the remains of Tethys Ocean activity in the study region. At the Early to Middle Jurassic boundary, the study region remained in an extensional tectonic setting with strong magmatic activity. The tectonic setting of the volcanic rocks of the Middle Jurassic Chara Formation and the Late Jurassic-Early Cretaceous volcanic rocks also indicates that the study region was in an extensional tectonic environment. During the middle and late Early Cretaceous, under the influence of subduction and a decrease in the crust, the study region developed shallow marine debris deposits of the Kebula Formation on the shore. During the Late Cretaceous, under the influence of the intensification of arc-continent collision and orogeny, and the disappearance of oceanic crust, the Zongzhuo Formation collapsed accumulation was formed.

7 Conclusion

(1) The volcanic rocks of the Sangxiu Group in the Zhegu area consist of basalt, dolerite, and volcanic breccia.
(2) The SHRIMP zircon U-Pb ages of the basalts of the Sangxiu Formation were 141 ± 1 Ma and 142 ± 1 Ma, and the diagenetic ages were Early Cretaceous.
(3) The Late Jurassic-Early Cretaceous volcanic rocks of the Sangxiu Formation, which are intraplate rifting products, originated from the mantle and were mixed with crustal materials. The rock type is intraplate alkaline basalt formed during the rifting activity of the passive continental margin extension.
(4) The Late Jurassic-Early Cretaceous Neo-Tethys Ocean was at a crucial stage of expansion. The expansion of the Late Triassic-Early Cretaceous Neo-Tethys Ocean was not a continuation of the expansion of the early Mid-Ocean Ridge, but a newer rifting of the passive continental margin. The Neo-Tethys Ocean has a multistage spreading nature.

Data availability statement

The original contributions presented in the study are included in the article/supplementary material, further inquiries can be directed to the corresponding authors.

Author contributions

FW and LW contributed to conception and design of the study. FW and JL conducted project administration. FW, JL, TY, and YT performed investigation. HX performed visualization and BC conducted supervision. All authors contributed to manuscript revision, read, and approved the submitted version.

Funding

This research was supported by the China Geological Survey Project (1212011220659 and DD20230479).

Acknowledgments

The authors thank Lidong Zhu and Shun Liu from Chengdu University of Technology for their help in manuscript preparation. They also thank their colleagues in the geological survey, and the reviewers for their helpful comments on an earlier draft of this paper.

Conflict of interest

The authors declare that the research was conducted in the absence of any commercial or financial relationships that could be construed as a potential conflict of interest.

Publisher's note

References

Cawood, P. A., Zhao, G. C., Yao, J. L., Wang, W., Xu, Y. J., and Wang, Y. J. (2018). Reconstructing South China in phanerozoic and precambrian supercontinents. *Earth-Sci. Rev.* 186, 173–194. doi:10.1016/j.earscirev.2017.06.001

Cheng, M., Lou, Y., Tang, Y., Liao, J., Chen, S., Li, Y., et al. (2022). Zircon U-Pb dating, geochemistry characteristics and tectonic implications of mafic dykes in the Chaiwa area, Southern Tibet. *Acta Petrol. Mineral.* 41 (3), 504–518.

Crame, J. A. (1996). A new oxytomid bivalve from the upper jurassic–lower cretaceous of Antarctica. *Palaeontology* 39 (3), 615–628.

Dong, S., Zhang, Z., Zhang, L., Li, G., Qing, C., Liang, W., et al. (2018). Geochemistry, Hf-Sr-Nd isotopes and petrogenesis of acidic volcanic rocks in Quzhuomu region of Southern Tibet. *Earth Sci.* 43 (8), 2701–2714.

Hodges, K. V. (2000). Tectonics of the Himalaya and southern Tibet from two perspectives. *Geol. Soc. Am. Bull.* 112 (3), 324–350. doi:10.1130/0016-7606(2000)112<324:tothas>2.0.co;2

Hryniewicz, K., Hagström, J., Hammer, O., Kaim, A., Little, C. T., and Nakrem, H. A. (2015). Late jurassic–early cretaceous hydrocarbon seep boulders from novaya zemlya and their faunas. *Palaeogeogr. Palaeoclimatol. Palaeoecol.* 436, 231–244. doi:10.1016/j.palaeo.2015.06.036

Jain, S. (2019). Middle Bathonian Indonesian macrocephalites cf. etheridgei (Spath) from SW Somalia. *J. Afr. Earth Sci.* 151, 202–211. doi:10.1016/j.jafrearsci.2018.11.021

Jiang, S., Nie, F., Hu, P., and Liu, Y. (2006). An important spreading event of the Neo-Tethys Ocean during the late jurassic and early cretaceous: Evidence from zircon U-Pb SHRIMP dating on diabase in nagarzê, southern Tibet. *Acta Geol. Sin.* 80, 522–527. doi:10.1111/j.1755-6724.2006.tb00272.x

Jiang, S., Nie, F., Hu, P., Liu, Y., and Lai, X. (2007). Geochemical characteristics of the mafic dyke swarms in South Tibet. *Acta Geol. Sin.* 81 (1), 60–71.

Jiang, W., Cao, K., Duan, X., He, X., Yin, P., Chen, J., et al. (2023). Influence of sedimentary environment evolution on fingerprint characteristics of methane isotopes: A case study from hangzhou bay. *J. Geophys. Res. Biogeosci.* 128, e2022JG007357. doi:10.1029/2022JG007357

Li, L. M., Lin, S. F., Xing, G. F., Davis, D. W., Davis, W. J., Xiao, W. J., et al. (2013). Geochemistry and tectonic implications of late Mesoproterozoic alkaline bimodal volcanic rocks from the Tieshajie Group in the southeastern Yangtze Block, South China. *Precambr. Res.* 230, 179–192. doi:10.1016/j.precamres.2013.02.004

Liu, Y. S., Hu, Z. C., Zong, K. Q., Gao, C. G., Gao, S., Xu, J. A., et al. (2010). Reappraisement and refinement of zircon U-Pb isotope and trace element analyses by LA-ICP-MS. *Chin. Sci. Bull.* 55 (15), 1535–1546. doi:10.1007/s11434-010-3052-4

Pál-Molnár, E., Batki, A., Ódri, Á., Kiss, B., and Almási, E. E. (2015). Geochemical implications for the magma origin of granitic rocks from the ditrău alkaline massif (eastern carpathians, Romania). *Geol. Croat.* 68, 51–66. doi:10.4154/gc.2015.04

Pearce, J. A., and Norry, M. J. (1979). Petrogenetic implications of Ti, Zr, Y, and Nb variations in volcanic rocks. *Contrib. Mineral. Petrol.* 69 (1), 33–47. doi:10.1007/bf00375192

Qiu, B. (2011). *New evidence of plume origin for the Comei fragmented large igneous Province in southeastern Tibet*. [dissertation]. [Beijing, China]: China University of Geosciences.

Sanematsu, K., Moriyama, T., Sotouky, L., and Watanabe, Y. (2011). Mobility of rare earth elements in basalt-derived laterite at the bolaven plateau, southern Laos: Mobility of rare earth elements in laterite. *South. Laos.* Resour. Geol. 61, 140–158. doi:10.1111/j.1751-3928.2011.00155.x

Tian, J., Ding, F., Hao, S., Pei, X., Li, T., Sun, Y., et al. (2021). Petrogenesis of acidic volcanic rocks in Sangxiu Formation, east-central segment of tethyan-himalaya: Response to break-up of eastern Gondwana continent? *Earth Sci.* 46 (11), 3926–3944. doi:10.3799/dqkx.2020.363

Tong, J., Liu, J., Zhong, H., Xia, J., Lu, R., and Li, Y. (2007). Zircon U-Pb dating and geochemistry of mafic dike swarms in the Lhozag area, southern Tibet, China, and their tectonic implications. *Geol. Bull. China.* 12, 1654–1664.

Tong, J., Zhong, H., Xia, J., Lu, R., and Yang, S. (2003). Geochemical features and tectonic setting of peraluminous granite in the Lhozag area, southern Tibet. *Geol. Bull. China.* 5, 308–318.

Vermeesch, P. (2006). Tectonic discrimination diagrams revisited. *Geochem. Geophys. Geosyst.* 7 (6), 466–480. doi:10.1029/2005gc001092

Xu, Z., Wan, S., Colin, C., Clift, P. D., Chang, F., Li, T., et al. (2021). Enhancements of himalayan and Tibetan erosion and the produced organic carbon burial in distal tropical marginal seas during the quaternary glacial periods: An integration of sedimentary records. *J. Geophys. Res. Earth Surf.* 126 (3), 1–17. doi:10.1029/2020JF005828

Zhong, H., Tong, J., Xia, J., Lu, R., and Qiu, J. (2005). Characteristics and tectonic setting of volcanic rocks of the Sangxiu Formation in the southern part of Yamzho Yumco, southern Tibet. *Geol. Bull. China.* 1, 72–79.

Zhu, D. C., Chung, S. L., Mo, X. X., Zhao, Z. D., Niu, Y., Song, B., et al. (2009). The 132 Ma Comei-Bunbury large igneous province: Remnants identified in present-day southeastern Tibet and southwestern Australia. *Geology* 37 (7), 583–586. doi:10.1130/g30001a.1

Zhu, D. C., Xia, Y., Qiu, B. B., Wang, Q., and Zhao, Z. D. (2013). Why do we need to propose the early cretaceous Comei large igneous province in southeastern Tibet? *Acta Petrol. Sin.* 29 (11), 3659–3670.

Zhu, D., Pan, G., Mo, X., Liao, Z., Jiang, X., Wang, L., et al. (2005a). Geochemistry and petrogenesis of the Sangxiu Formation basaltsin the central segment of tethyan himalaya. *Geochimica* 34 (1), 7–19.

Zhu, D., Pan, G., Mo, X., Liao, Z., Jiang, X., Wang, L., et al. (2007). Petrogenesis of volcanic rocks in the Sangxiu Formation, central segment of tethyan himalaya: A probable example of plume–lithosphere interaction. *J. Asian Earth Sci.* 29 (2-3), 320–335. doi:10.1016/j.jseaes.2005.12.004

Zhu, D., Pan, G., Mo, X., Wang, L., Liao, Z., Jiang, X., et al. (2005b). SHRIMP U-Pb zircon dating for the dacite of the Sangxiu Formation in the central segment of Tethyan Himalaya and its implications. *Sci. Bull.* 50 (6), 563–568. doi:10.1360/04wd0281